

International Conference on Space Optics—ICSO 2012

Ajaccio, Corse

9–12 October 2012

Edited by Bruno Cugny, Errico Armandillo, and Nikos Karafolas



Weighing supermassive black holes with the UV photon sieve space telescope

Vladimir Airapetian

Robert S. Upton

Joseph Davila

Marzouk Marzouk

et al.



Weighing Supermassive Black Holes with the UV Photon Sieve Space Telescope

Vladimir Airapetian
Sigma Space Corporation
Lanham, Maryland,
USA 20706

Email: vladimir.airapetian@sigmaspace.com

Robert S. Upton
Sigma Space Corporation
Lanham, Maryland,
USA 20706

Email: Robert.Upton@sigmaspace.com

Joseph Davila
NASA Goddard Space Flight Center
Greenbelt, Md, USA
Email: joe.davila@nasa.gov

Marzouk Marzouk
Sigma Space Corporation
Lanham, Maryland,
USA 20706

Email: Joe.Marzouk@sigmaspace.com

Kenneth G. Carpenter
NASA Goddard Space Flight Center
Greenbelt, Md, USA
Email: kenneth.g.carpenter@nasa.gov

Kimberly Weaver
NASA Goddard Space Flight Center
Greenbelt, Md, USA
Email: kimberly.weaver@nasa.gov

Abstract—The Photon Sieve Space Telescope (PSST) is a space-based ultra high-resolution (5 mas) narrow band ($\lambda/\Delta\lambda \simeq 1000$) spectral UV imager providing spectral imaging of astronomical objects in $Ly - \alpha$, CIV and NV emission lines. Science obtained with this telescope will revolutionize our understanding of a whole range of astrophysical processes in the local and distant universe. There will be a dramatic increase in the number of observed moderate and large SMBH masses as well as extra-solar protoplanetary disks. The observations will also enable tracing the star formation rates in active galaxies. We present the optical design, the properties and the future implementation of the proposed UV photon sieve space telescope.

I. INTRODUCTION

Recent high spatial resolution observations of the local and distant Universe have opened new avenues in astrophysics. It is important to optimize telescope instrumentation for space-based UV and X-ray observations because the Earth's atmosphere limits the bands observable with ground-based telescopes. This trend is already in place with proposed launch of the *James Webb Space Telescope* (JWST)[1] that will perform observations of the Universe in the mid-infrared band. Space based telescopes are also desirable because they experience little of the thermal and gravitational structural flexure of ground-based telescopes. The relative stability of the space telescope point spread function, and its ability to track an object over many hours makes space based UV astronomy a necessity. The current and projected technological capabilities of high precision mirror polishing cannot provide mirrors with sufficiently accurate figures without overly burdensome lead-time and cost. We propose a feasible method that can result in high spatial and wavelength resolution imaging of UV processes in the Universe.

In recent years researchers suggested that a photon sieve (PS), a novel version of the Fresnel zone plate (FZP), may provide a viable opportunity to reach diffraction limit in X-ray imaging [2]. A photon sieve (PS) is essentially a FZP with an array of circular holes replacing the open zones, as

shown in Fig. 2. [3] developed the theory for calculating the distribution of light in the focal plane for an arbitrary PS. Photon sieves have been fabricated and tested in visible light [4], [5] and suggested for UV and X-ray imaging [6], [7]. Due to their extremely high resolution, they have also been considered for imaging exoplanets [8], [9], [10]. The major reasons behind recently enhanced attention to photon sieves are their relatively low fabrication costs, the capability to manufacture large aperture lightweight diffraction optics, and the relative insensitivity of the PS to manufacturing errors, which enables them form diffraction limited images in the presence of state of the art manufacturing errors.

In this paper we present a new design for a 5-meter PS that will perform UV spectral imaging of active galaxies (hereafter called active galactic nuclei or AGN) in the nearby and distant Universe. We also present scalar wave diffraction simulation results for a small scaled PS, and we present some art-work for a segmented PS aperture that is feasible for large format photon sieve space telescopes (PSST).

II. SCIENCE ENABLED BY THE UV PHOTON SIEVE SPACE TELESCOPE

Determining the mass of the central black hole in galaxies is a question of fundamental importance in the modern astrophysics, allowing measurement of the efficiency of radiation (the so-called Eddington ratio), the relationship of the black hole to its host galaxy and the connection between the two, which has influenced the growth of structure in the universe via feedback. It has long been realized [11] that a significant fraction of radiating super-massive black holes (SMBH) in the centers of AGNs are surrounded by gas which is ionized by the AGN and whose dynamics are controlled by Keplerian motion. Spatially and spectrally resolved measurements of this gas [12]; [13] can determine of the mass of the black hole. However the limited spatial resolution and sensitivity of Hubble space telescope (HST) (about 60 mas) has limited

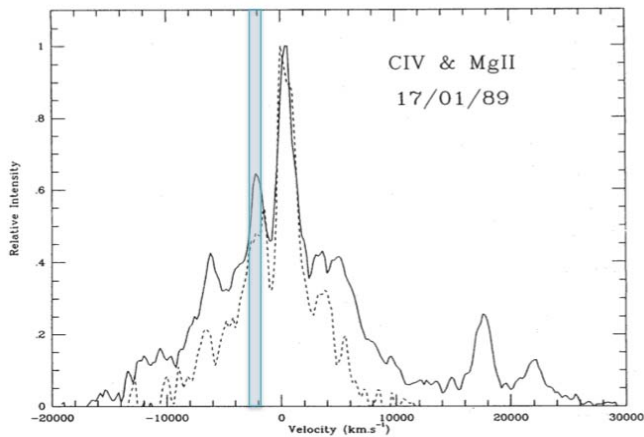


Fig. 1. Scanning across velocity - broadened line profiles will allow the PSST to measure velocity fields for AGN and thus measure black hole mass.

the derivation of such masses with this technique to only 17 objects [14].

The technical requirement to measure black hole mass is set by effect of the potential well on the dynamics of the gas surrounding it. We could vastly increase the number of known SMBH masses by dynamically measuring the velocity widths of UV emission lines from the broad line region (BLR). Driven by requirements to resolve BLRs for many AGNs to a linear scale of less than 1 pc, we must image structures at a resolution of at least 5 mas in a 1 Å band in UV lines such as O VI λ1032/1038 Å, N V λ 1238/1242 Å, Ly λ1216 Å, C IV λ 1548/1550 Å. This is to study evolution of masses in early universe we will sample AGNs at z=0 (the current epoch) to at least z=1.3 (8 billion years ago). To sample the kinematics of AGNs and thus determine masses of SMBH within a 50 Mpc radius, we require the angular resolution of 5 mas. This is 10 times greater than HST's resolving power.

We have recently developed the Photon Sieve Space Telescope (PSST) concept presented in section III, which will be able to resolve linear structures in nearby galaxies to less than 10 pc and at z=1 to less than 100 pc. The properties of the PSST enables narrow band (about 1 Å) spectral imaging of astronomical objects in different parts of a selected UV spectral line. The subsequent scanning of an image across the spectral line profile will directly probe the motions of plasma that can be observed in regions of astronomical interest (as illustrated in Figure 1), including the regions associated with disk accretion, radial infall and/or outflows.

III. THE PHOTON SIEVE TELESCOPE

The photon sieve telescope (PST) contains a screen with a concentric pattern of holes drilled into it. The diameter of the holes varies with radial position in the screen. The holes are nominally located in Fresnel zones[15], [16] that are located in annular radial zones nominally perpendicular to the Poynting

vector[15]¹

A. Fresnel diffraction theory

According to Fig. 2, the wavefield emanating from a point source that arrives at the radial zonal location r_n of PST aperture has its Fresnel zones that are separated by $2m\pi$ radians come to a focus at the distance q behind the screen according to Eq. (1).

$$k \frac{r_n^2}{2q} = 2m\pi. \quad (1)$$

The value m is the *Fresnel zone number*, is the number of Fresnel zones in the beam, and varies with propagation distance ($z \simeq q$) from the aperture, wavenumber $k = \frac{2\pi}{\lambda}$, and zone location ($r_n = \sqrt{x_n^2 + y_n^2}$). The value of m is undefined at focus, yet it encapsulates the diffraction properties of the wave fields near focus and is written as,

$$m = \frac{w^2}{4\lambda z}. \quad (2)$$

Where w is the diameter of the outer diffraction aperture shown in Fig. 2.

The diameter of the zone (w_n) in the screen that results in constructive interference of the wavefields at focus (q) varies as,

$$k \frac{w_n r_n}{q} = 2\pi. \quad (3)$$

The coherent wave field at the focal point q from the photon-sieve (PS) is constructed by a coherent superposition of diffracted fields $U_n(X, Y)$ from the aperture (x, y) shown in Fig. (2) that were incident upon the focal plane (X, Y) . The focal plane field $U_n(X, Y)$ is related to the aperture $U_n(x, y)$ by the Fresnel diffraction integral[16], [3],

$$U_n(X, Y) = \frac{A_n}{\lambda q} \int_{\Omega} \int_{\Omega} U_n(x, y) \exp \left[-ik \frac{(X-x)^2 + (Y-y)^2}{2q} \right] dx dy. \quad (4)$$

The phase relation in Eq. (4) is easily transformed into spherical polar coordinates, with the resultant integral in Eq. (4) now expressed as a zeroth-order Hankel transform[17],

$$U_n(\rho') = \frac{\pi A_n}{\lambda q} \exp \left[ik \frac{R'^2}{2q} \right] \int_{\Omega} \exp \left[ik \frac{r'^2}{2q} \right] J_0 \left[\frac{kr' \rho'}{q} \right] r' dr' \quad (5)$$

The properties of the focal plane irradiance distribution is evaluated by introducing a parabolic phase front into the pupil field,

$$U_n(x, y) = \exp \left[ik \frac{x^2 + y^2}{2q'} \right]. \quad (6)$$

The variation of the normalized on-axis irradiance as a function of axial position along the direction of focus is shown in Fig. (3). The variation of the normalized on-axis irradiance as a function of axial position along the direction of focus is shown in Fig. (3).

¹The Poynting vector $\langle \mathbf{S} \rangle = \langle \mathbf{E} \times \mathbf{H} \rangle$ in the vector treatment of electro-magnetic waves is qualitatively similar to the Eikonal equation $\nabla L = \frac{dW}{ds}$, which is perpendicular to the propagating wavefront.

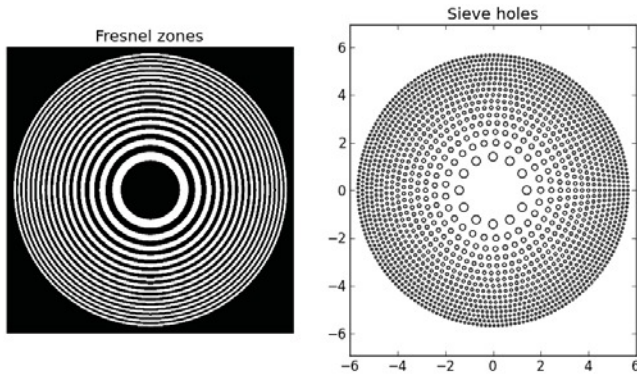


Fig. 2. The Fresnel zone plate (FZP) for an 12 mm diameter aperture, focal length 1m, for wavelength $1 \mu m$. The radial value r_n of the first zone is shown. The Fresnel zone construction for propagating wavefronts arises from the Huygens-Fresnel principle, which states that the propagating wave field can be treated as a coherent superposition of spherical wave fields. The FZP can be constructed by the photon sieve holes located in the white zones, as shown in the right figure. In the limit of many holes, the *point-spread function(s)* (PSF(s)) are identical for the FZP and photon sieve. The example shown here is a small scale and is included as a demonstration of the principle.

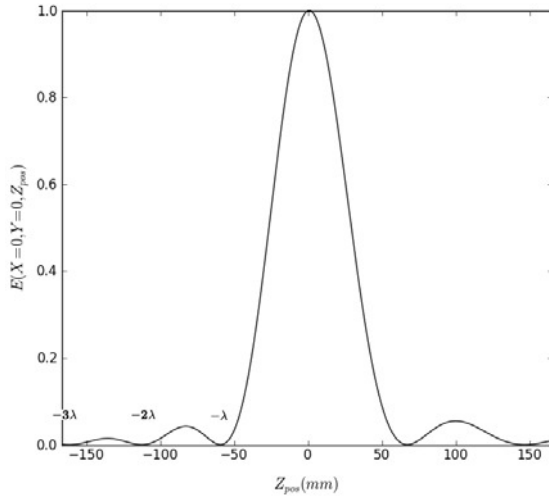


Fig. 3. The variation of the normalized on-axis irradiance with focal position Z_{pos} . The minima before and after focus correspond to where there are an even number of Fresnel zones in the beam, i.e. when the Fresnel number is even, which corresponds to whole numbers of waves of defocus error in the beam. The minima in the on-axis irradiance before focus are annotated with the amount of focus $-\lambda, -2\lambda, -3\lambda$. In the general case the axial irradiance variation is not symmetric about focus (nominally where $zPos = 0$). The axial irradiance is calculated for the PST aperture shown in Fig. 2.

The properties of the focal plane irradiance distribution have to be properly modeled to optimize the amount of focus diversity[18] introduced to the focusing field in order to adequately perform the phase reconstruction of the pupil to provide optical control of the PST. The inside and outside irradiances $\mathbf{E}_{in}(X, Y; -z)$ and $\mathbf{E}_{out}(X, Y; +z)$ are introduced into the cost function ϵ in Eq. (7) that is optimized with respect

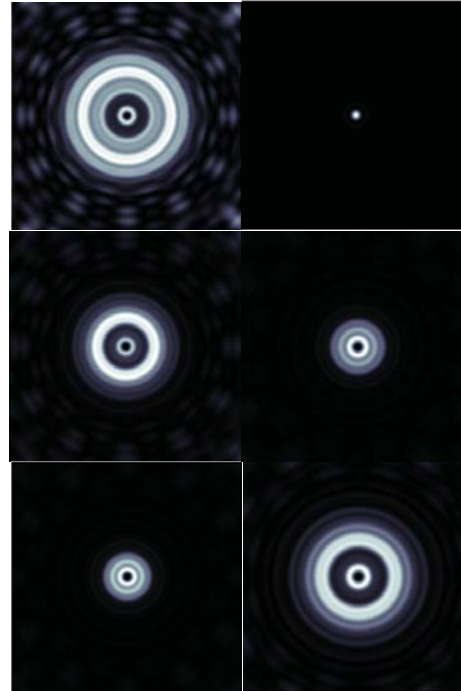


Fig. 4. The irradiance distributions corresponding to defocus positions from focus along the propagating axis of the diffracting beam. The irradiance distributions are arranged in the order indicated in Fig. 3. That is, the $-3\lambda, -2\lambda,$ and $-\lambda$ defocus irradiance values are arranged along the left column, and the $0, +\lambda,$ and $+2\lambda$ defocus radiance values are arranged along the right column. Comparison between the complementary $-2\lambda,$ and $+2\lambda$ and $-\lambda,$ and $+\lambda$ focus positions have similar qualitative properties, but are different, which is consistent with Fig. 3.

to the Zernike[15] phase terms contained in $U_n(x, y)$ Eq. (4).

$$\epsilon = \int_{X,Y} [\mathbf{E}_{in}(X, Y; -z) - psf_{in}(X, Y; -z)]^2 dXdY + \int_{X,Y} [\mathbf{E}_{out}(X, Y; +z) - psf_{out}(X, Y; +z)]^2 dXdY(7)$$

The complex field distribution from the near-field region to the far-field region within the first Fresnel zone focus is calculated from quasi-analytic code written in *Python*[19] with *Scipy*[20], *Numpy*[21], and *Matplotlib*[22] modules.

B. Photon-Sieve Telescope: Optical Design

The PSST is characterized by the selection of three parameters: the wavelength, (λ), the diameter of the outer zone², D , and the width of the outer zone, Δ . The reference wavelength is centered on $Ly - \alpha$ emission line. The diameter is chosen to provide the necessary spatial resolution to image the features of interest, and the width of the outer zone is generally set by fabrication considerations and detector pixel size considerations (see specifications in Table 1). The PSST is planned to be deployed in a formation flying configuration with two spacecraft around the L2 Sun-Earth Lagrangian point and controlled by micro-thrusters for flying and repointing.

²The outer zone diameter is equal to $2r_n$ for n as a maximum.

TABLE I

OPTICAL DESIGN OF THE PSST IN THE UV BAND AROUND $Ly - \alpha$.

Parameter	Value
Diameter	500 cm
Spectral bandwidth	1 \AA
Number of zones	1000
Spot size	1.25 mm
Focal length	42 km
Rayleigh resolution	5 mas
Depth of focus	26.04 m
Diameter of the smallest pinhole	1.9125 mm
Field of view	2 arc-sec
Size of the detector	152.5 mm x 152.5 mm

One spacecraft will carry the photon sieve and another will be carrying the UV imaging detector, to be located at variable distances from the photon sieve. The focal length of the PSST is dependent on the wavelength of a spectral line and this will be achieved by mutual motions of the two spacecraft. Adjusting the focal length to be less than 42 km will allow observations of in galaxies with redshift of $z=1$ and greater. With a throughput of about 10%, the light collecting area of the 5-meter PSST is about 43% of HST's, but the resolution at $Ly - \alpha$ is 5 mas, which is 10 times better than HST.

Pointing information will be updated frequently to provide sufficient bandwidth to negate instrument jitter. In addition to image motion compensation, this mount will provide focus adjustment and wavelength scanning capabilities by incorporating axial motion. We will use the chromatic focus of the photon sieve to our benefit by scanning the focus on the detector, and thereby scanning in wavelength.

Our prototype ground-based PS telescope will contain up to 18 hexagonal segments. The segments will be fit together to form the aperture, as shown in Fig (5). The segments will have three different prescriptions with the segments in a given hexagonal ring having the same prescription. The segments are used to demonstrate segment phasing and verify PSST sensitivities to optical control residual misalignments.

IV. CONCLUSION

The UV PSST described in this paper will provide a new way to probe the masses of SMBH in nearby and distant (up to $z=1.3$) active galaxies and thus shed light on the evolution of AGNs and their environments in the second half of the history of the Universe. These science goals can be achieved by the unique properties of the UV photon sieve imager with the aperture of 5 m that will provide 5 mas resolution in narrow spectral bands ($\sim 1 \text{ \AA}$) within broad UV spectral emission lines such as $Ly-\alpha$, CIV and NV forming in the vicinity of SMBHs.

We calculated the PSF for a small aperture PS as an example. Larger PSST apertures can be manufactured to form hexagonal fitted mirrors, such as those illustrated in Fig. 5. In the case of segmented aperture telescopes, like that shown in Fig. 5, the segments will have to be phased to within the coherence length of the source. This can be accomplished by means of focal plane-based wavefront sensing and optical

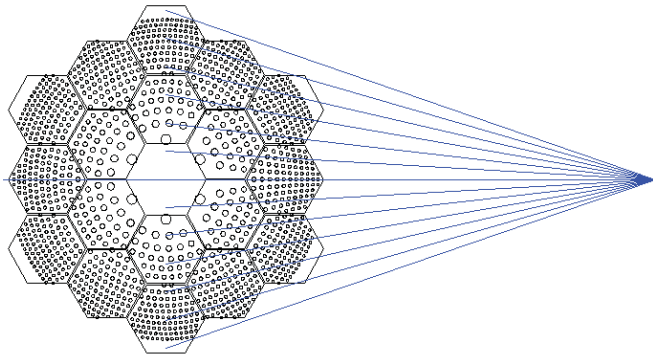


Fig. 5. The model PST aperture with aperture segments included. The model is rendered in Zemax[23] with rays traced to simulate the propagation of wave fields from the entrance aperture to the focal plane. For space telescope missions that require 2 m or greater apertures, the segmented approach is a practical and versatile solution that allows for packaging of the telescope in rocket faring, as well as the manufacture of smaller stiff aperture plates the size of each segment, rather than the manufacture of a single monolithic plate.

control techniques. In order to optimize the optical control and wavefront sensing parameters a full analysis of the focal plane irradiance distribution is required, which will also include the optical signals from other wavelength components that vary along the optical axis.

ACKNOWLEDGMENT

The authors would like to thank Dr. Richard Mushotzky (University of Maryland at College Park) and Ms. Sevinc Figen Oktem (University of Illinois Urbana-Champaign Department of Electrical Engineering) for their valuable input and participation in this effort.

REFERENCES

- [1] Gardner, J. P., Mather, J. C., Clampin, M., et al. 2006, Springer, 123, 485.
- [2] Kip, D., Anastassiou, C., Eugenieva, E., Christodoulides, D., & Segev, M. 2001, Optics Letters, 26, 524(2001)
- [3] Cao, Q. & Jahns, J., 2002, J. Opt. Soc. Am. A, Vol. 19, No. 12.
- [4] Anderson, G., 2005, Opt. Lett. 30 (22), 2976.
- [5] Anderson, G., 2010, Appl. Opt., 49(33), 6391.
- [6] Davila, J. 2011, Proc. of the SPIE, 8148, 814800
- [7] Gorenstein, P., 2006 SPIE Newsroom, 10.1117/2.1200601.0011.
- [8] Koechlin, L., Serre, D. & Duchon, P., 2005, A&A, 443, 709.
- [9] Koechlin, L., Serre, D. & Deba, P., 2009, A&SpSci, 320, 225.
- [10] Hinglais, E., 2011, Exp. Astron, 30, 85.
- [11] Harms, R. J., Ford, H. C., Tsvetanov, Z. I., et al. 1994, Ap. J, 435, L35
- [12] Bower, G. A., Green, R. F., Danks, A., et al. 1998, Ap. J, 492, L111
- [13] Ferrarese, L., Ford, H. C., & Jaffe, W. 1996, Ap. J, 470, 444
- [14] Ferrarese, L., & Merritt, D. 2000, Ap. J, 539, L9
- [15] M. Born and E. Wolf, *Principles of optics*, 6th ed. Pergamon Press, 1993.
- [16] J. Goodman, *Introduction to Fourier optics*, 2nd ed. McGraw-Hill, 1988.
- [17] Ronald N. Bracewell, 1986, *The Fourier transform and its applications*, 2nd ed. McGraw-Hill. p. 247.
- [18] Gonsalvez, R. A., 1982, Opt. Eng. 21, No. 5.
- [19] www.python.org.
- [20] www.scipy.org.
- [21] www.scipy.numpy.org.
- [22] www.matplotlib.sourceforge.net.
- [23] Zemax is a commercially available optical design and modeling software code available from www.zemax.com.